arXiv:1610.00437v1 [cond-mat.supr-con] 3 Oct 2016

Current Induced resistive state in Fe(Se,Te) Superconducting Nanobridges

C. Nappi,[1,*] C. Camerlingo,[1] E. Enrico,[2] E. Bellingeri,[3]
V. Braccini,[3] C. Ferdeghini,[3] and E. Sarnelli[1]

[1]*CNR-SPIN, Sezione di Napoli, I-80078 Pozzuoli, Napoli (NA), Italy*
[2]*INRIM, Istituto Nazionale di Ricerca Metrologica, I-10135 Torino, Italy*
[3]*CNR-SPIN, Genova, Corso Perrone 24, I-16152 Genova, Italy*

(Dated: October 4, 2016)

Abstract

We study the current-voltage characteristics of Fe(Se,Te) thin films deposited on CaF_2 substrates in form of nanostrips (width $w \sim \lambda$, λ the London penetration length). In view of a possible application of these materials to superconductive electronics and micro-electronics we focus on transport properties in small magnetic field, the one generated by the bias current. From the characteristics taken at different temperatures we derive estimates for the pinning potential U and the pinning potential range δ. Since the sample lines are very narrow, the classical creep flow model provides a sufficiently accurate interpretation of the data only when the attractive interaction between magnetic flux lines of opposite sign is taken into account. The observed voltages and the induced detriment of the critical current of the nanostrips are compatible with the presence of few tens of magnetic field lines at the equilibrium and a strongly inhomogeneous current density distribution. In particular, we argue that the sharp corners defining the bridge geometry represent points of easy magnetic flux lines injection. The results are relevant for creep flow analysis in superconducting Fe(Se,Te) nanostrips.

PACS numbers:

*Electronic address: ciro.nappi@spin.cnr.it

Introduction

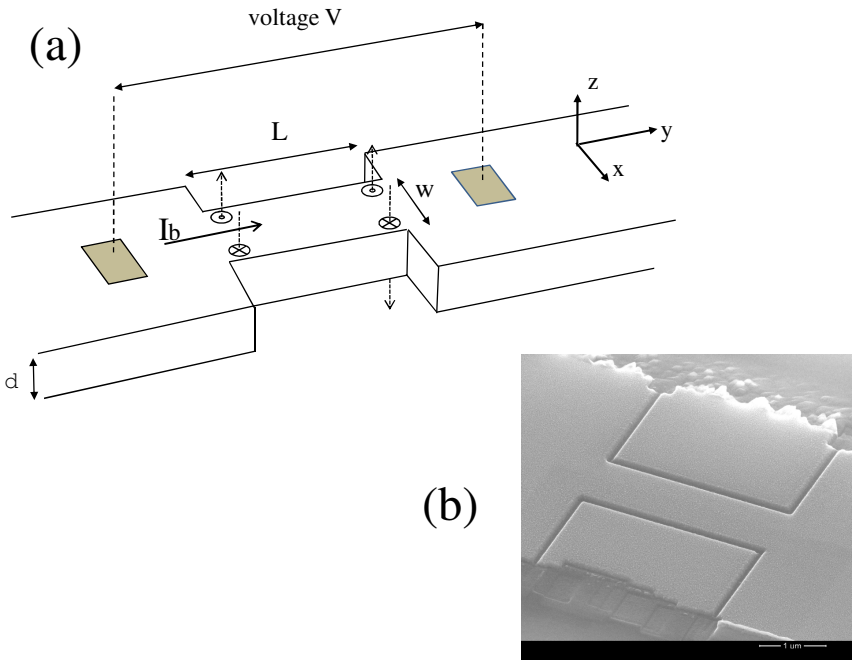

FIG. 1: (a) Geometry of the nanostrips used in this work. Also shown schematically the self-generated magnetic field lines entering the sample in the presence of a current bias I_b. (b) a SEM photograph of sample B (w = 800 nm).

Currently, iron based superconductors are object of intense investigations concerning their fundamental properties[1–10]. A potential use of these materials is in the field of large scale current transport [11]. However, as is well known, the presence of mobile magnetic flux lines in superconductor samples affects their current transport properties even when a magnetic field is not expressly applied [12]. In this case the magnetic field self-generated by the bias current is able by itself to create magnetic vortices that, when in motion, induce dissipation in the sample under test. According to the creep flow model [13] the degree of dissipation in a superconducting film, for a fixed current density, depends on the pinning potential U of the film and on the density of pinning sites. For electronics and nano-electronics applications of new superconducting materials, like the recently discovered iron based pnictides and chalcogenides superconductors, the study of the pinning energy

and the current transport under condition of weak magnetic field is of fundamental interest since the magnetic field experienced by the films (which are patterned in the form of submicron strip-lines) is as low as few tens of gauss in those applications. From this point of view, these investigations are analogous for primary relevance to those carried out under conditions of high magnetic fields, when the research perspective is the employment of these materials for high power applications [14–18]. With these motivations in mind, in this work we have investigated the current induced resistive state of narrow (width $< 1\mu$m) Fe(Se,Te) iron-chalcogenide nanostrips. The current-voltage characteristics have been measured at different temperatures $T < T_c$ (T_c is the superconductor critical temperature), at sub-critical current values ($I_b < I_c(T)$) and in the absence of an externally applied magnetic field. We show that the experimental results can be qualitatively explained on the basis of a flux depinning model of quasi-isolated vortices. A pinning energy of order of few tens of meV, as well as a pinning range of few nanometers, are estimated, compatible with defects extending along the film thickness. Although the analysis carried out with conventional flux creep models in zero external field [19–21] qualitatively account for the observed features, an important corrective term, proportional to λ/w, must be introduced for improving the accuracy of the pinning energy estimate. This correction stems from the very narrow width of the sample under test. The element to consider necessarily is the attractive Lorentz-like force exerted between magnetic vortex lines of opposite sign entering the two close opposite edges (vortex-antivortex interaction). This force usually is negligible in large width samples ($w \sim 10\lambda$ or larger) because the self-generated magnetic flux lines are sufficiently separated most of their life time while crossing the strip. On the contrary, in narrow strips ($w \leq \lambda$) at sub-critical bias currents, this force may be as intense as the Lorentz force. Nevertheless, even with the introduction of this correction, the resulting pinning energy is lower than the one reported in literature for Fe(Se,Te) in the presence of intense magnetic fields [17].

Results

For the measurements of the current-voltage characteristics (CVCs), a Fe(Se,Te) film with thickness $d = 100$ nm was patterned in the form of nanostrips with length $L = 3$ μm and

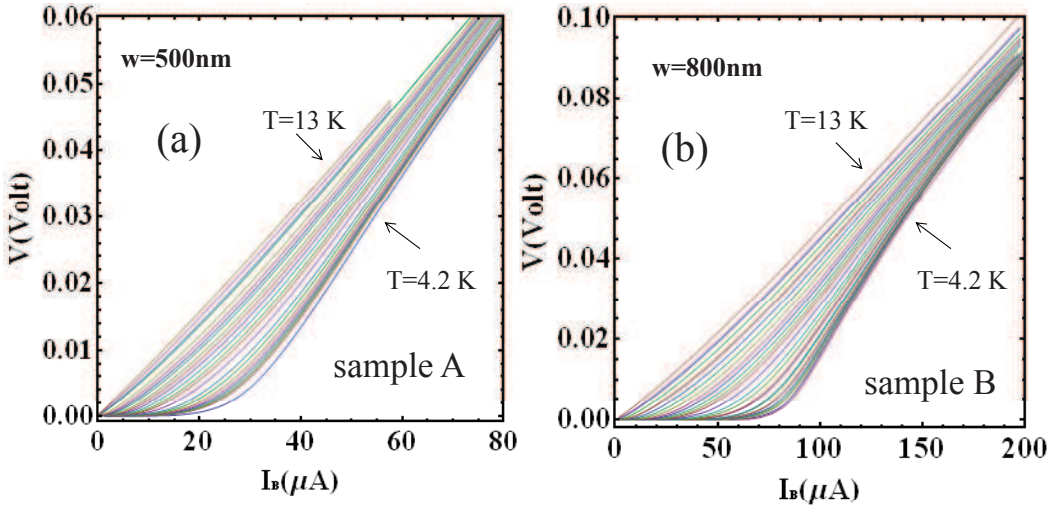

FIG. 2: Current voltage characteristics:(a) Sample A, w=500 nm. (b) Sample B, w=800 nm for different temperatures.

Sample	$L(\mu\text{m})$	w(nm)	T_c(K)	j_c[4.2 K](A/cm^2)
A	3	500	13	3.2×10^4
B	3	800	13	8.1×10^4

TABLE I: Parameters of the nanostrips.

width $w = 500$ nm (sample A) and $w = 800$ nm (sample B), respectively. Fig. 1 illustrates the geometry of our Fe(Se,Te) nanostrips, while Table I summarizes the experimental sample parameters. The critical current densities of sample A and B at $T = 4.2$ K, i.e. $j_c = 3.21 \times 10^4$ and $j_c = 8.1 \times 10^4$ A/cm^2, respectively, are one order of magnitude lower than the Fe(Se,Te) bulk value. The slight reduction found in sample A, as compared with sample B, is probably to due to the detrimental of superconductivity properties caused by the etching process. However the extrapolated current density at $T = 0$ (see next section) gives the common value

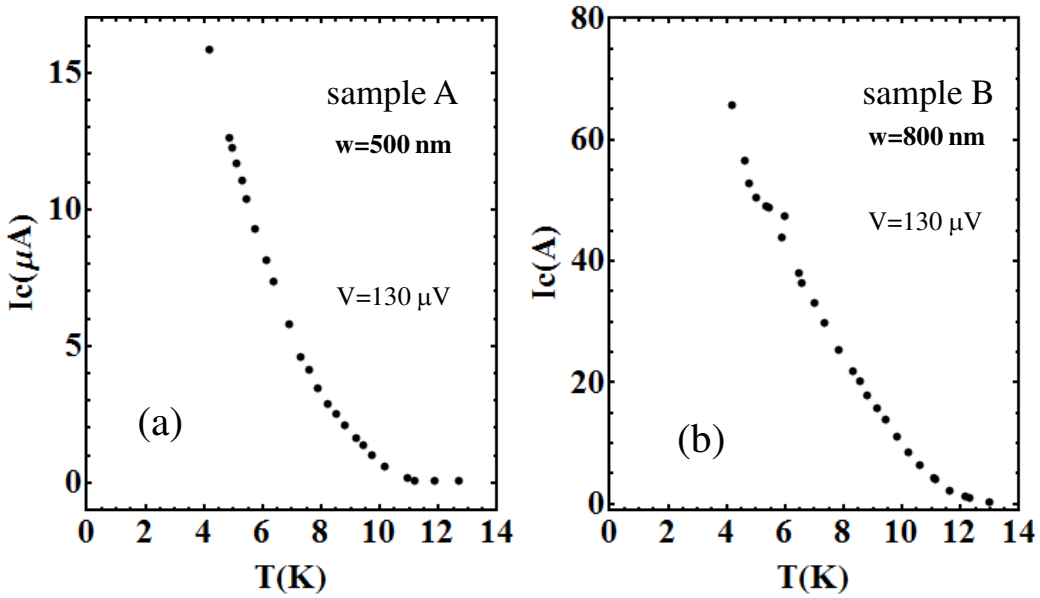

FIG. 3: Temperature dependence of the critical current I_c (The current at which the voltage $V = 130$ μV appears across the nanostrips) for (a), sample A and (b), sample B

of $j_c \sim 1.5 \times 10^5$ A/cm^2 in both samples. CVCs were collected at different temperatures between 4.2 K and 13 K for the two samples, A (24 curves) and B (27 curves), and are shown in Fig. 2. The measured curves, when considered in the full range of currents, extrapolate to zero showing zero excess current. As can be seen the CVCs show appearance of resistivity at finite temperatures, well below T_c at small bias current density, a feature that we attribute to creep flow, i.e. to vortex depinning processes. Hereafter, we will assume the following parameters for the superconductor: London penetration depth $\lambda(0) = 560$ nm, coherence length $\xi(0) = 2$ nm ($Fe_{1.03}(Te_{0.63}$ $Se_{0.37}$) [22]; upper critical field $B_{c2} \sim 100$ T [14, 23], in a fair agreement with the theoretical estimate [24] $B_{c2} = \phi_0/2\pi\xi^2 = 80$ T. In Fig. 3, the experimental dependence of the critical current on the temperature is shown. The critical current $I_c(T)$ decreases, far from T_c, almost linearly with the temperature (we here conventionally define $I_c(T)$ as the current at which the voltage $V = 130$ μV appears across

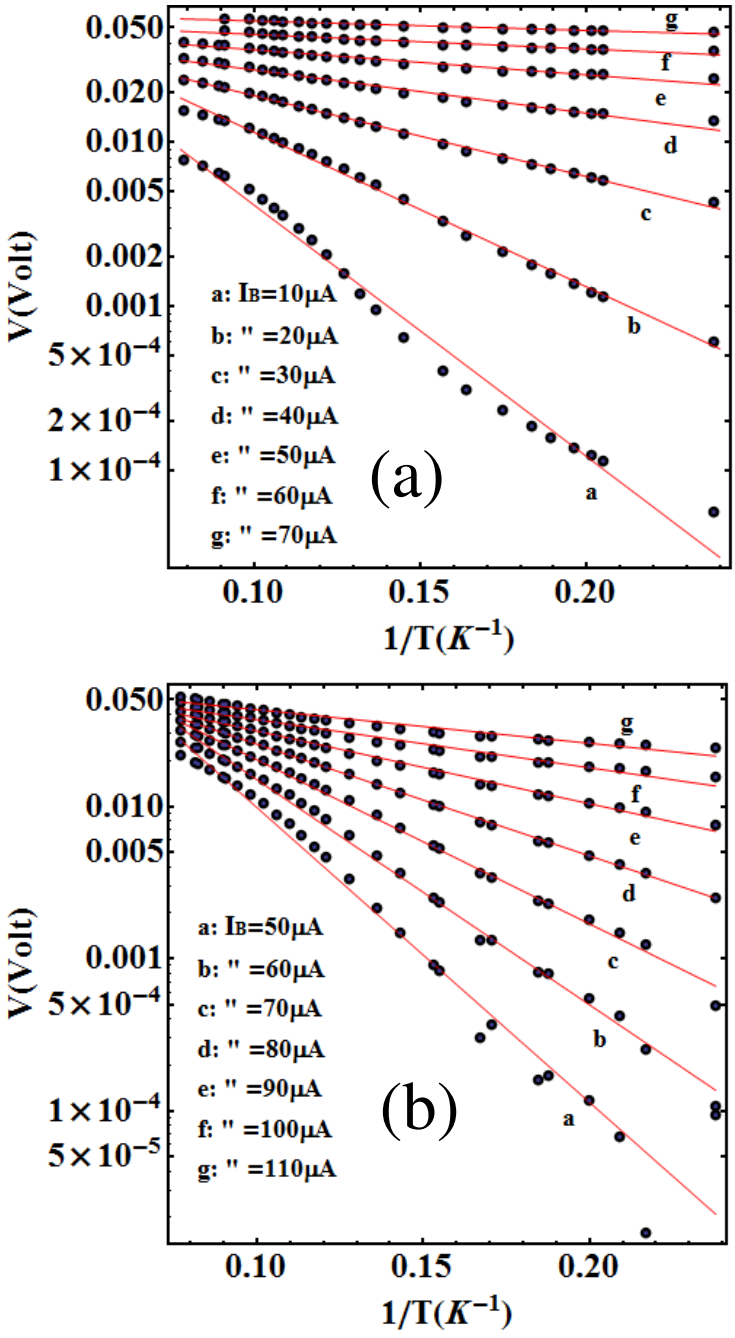

FIG. 4: Inverse of the temperature dependence of the voltage when the sample ((a), sample A and (b), sample B)) is current-biased ($\log(V) - 1/T$ relation) as obtained from data in Fig. 2. Almost linear dependence of log(V) on 1/T is observed consistently with the theoretical flux creep model, equation (9) (solid lines).

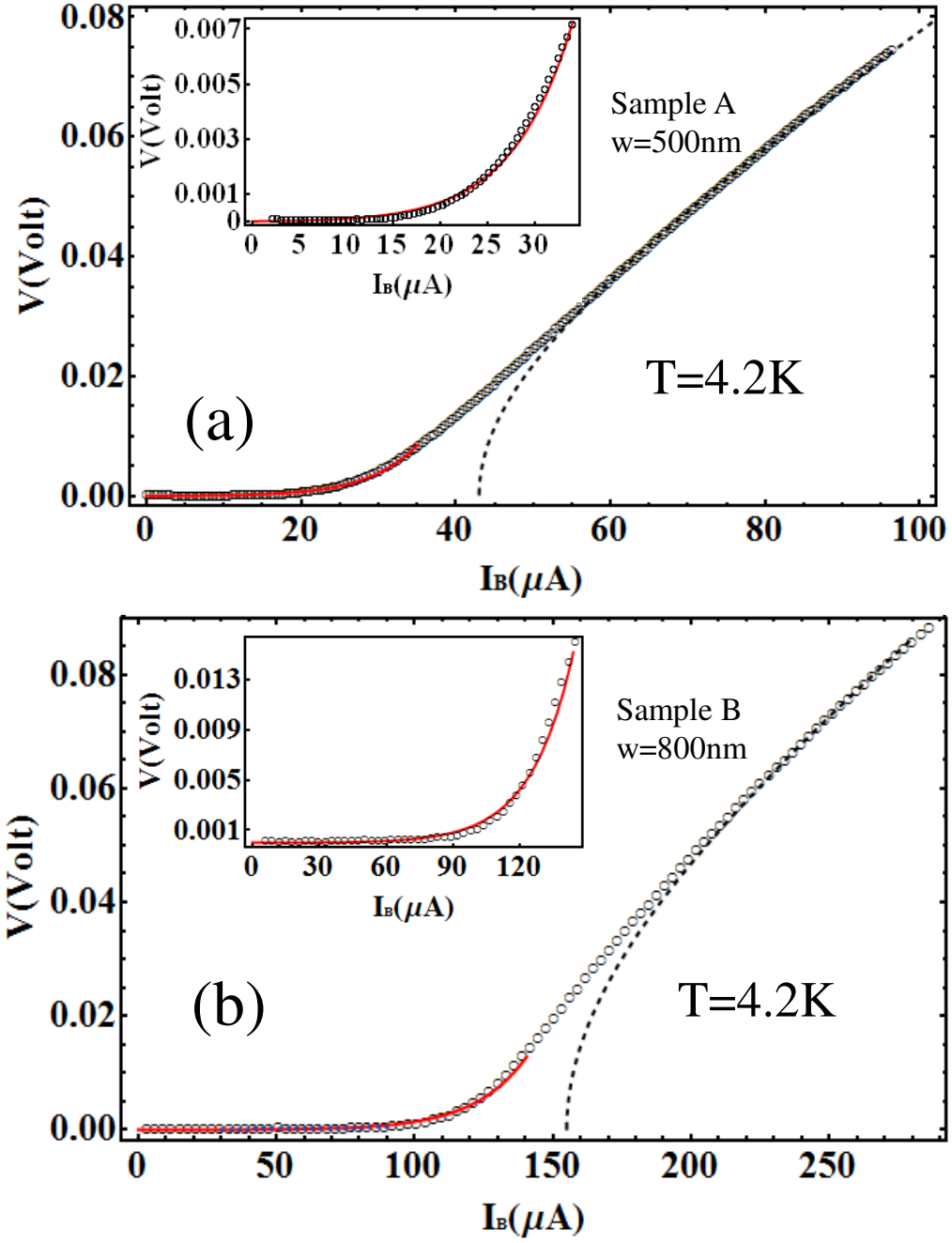

FIG. 5: (a) Current voltage characteristics @T=4.2 K of sample A (w=500 nm) and (b) sample B (w=800 nm). The red line is the creep flow function $V = R_{cf} I_b \exp(I_b/I_0)$. (a) $R_{cf} = 2.66\ \Omega$ and $I_0 = 8.29\mu$ A; (b) $R_{cf} = 0.15\ \Omega$ and $I_0 = 21.9\ \mu$A. Insets show the detail of the flux creep fit. The dashed lines at high bias currents are the flux flow theory fits of the experimental points.

the Fe(Se,Te) nanostrips). This dependence of the critical current on the temperature agrees with the interpretation in terms of creep flow of our data set [25]. Furthermore, in Fig. 4 we show experimental results of the $\log(V) - 1/T$ relation (the Arrhenius plot) when sample A and sample B are current biased for the bias current values indicated in the legend. As can be seen the value of $\log(V)$ decreases linearly with 1/T, which is consistent with the creep flow interpretation and the theoretical predictions of equation (8) or (9).

Creep flow, studied in literature chiefly in the presence of an external magnetic field [7, 14–18], is a manifestation of the thermal agitation of the magnetic flux lines as they are acted upon, in the same time, by the adhesion force to crystalline defects and by the Lorentz force. In contrast, the term "flux flow" designates the viscous motion of quasi-free magnetic flux lines driven by the Lorentz force at higher bias currents where the effect of pinning is negligible. Roughly speaking, the two phenomena manifest themselves in the CVC as strongly non linear and linear parts of the current-voltage plot, respectively. Fig 5, as an example of the relevance of this classification for our CVC data, shows the CVC at T = 4.2 K of the sample A (5a) and sample B (5b),respectively. The red line is the creep flow model fit of the experimental points (black dots) at low currents (see the insets of Fig. 5, a) and b)). The creep flow fitting expression used in plot is $V = R_{cf} I_b \exp(I_b/I_0)$, where R_{cf} and I_0 are fitting parameters whose meaning will be discussed in the next section. The dashed line at high currents in the same plot is the flux flow fit of the data. The fitting expression used for this part of the plot is $V = R_{ff}\sqrt{(I_b^2 - I_{cff}^2)}$[26], with $R_{ff} = 860\Omega$ and $I_{cff} = 43\mu$A (Sample A) and $R_{ff} = 370\Omega$, $I_{cff} = 155\mu$A (Sample B). Here I_{cff} has the meaning of an estimate superconducting critical current in the sample which is free of flux creep in the presence of pinning. The quantity R_{ff} is the resistance of the nanostrips, arising because of the viscous motion of magnetic flux. In this work we will focus on the non-linear part of the current voltage characteristic observed at lower currents.

Review of the creep flow model equations and discussion

Single Vortex Model Creep

The bias current injected in the superconductor nanostrips generates a self-field that limits the effective critical current density j_c of the nanostrips. For a type II superconductor, the relevant critical field at which this dissipative condition starts is the lower critical field: [24]

$$B_{c1}(T) = \mu_0 H_{c1}(T) = \frac{\phi_0}{4\pi\lambda(T)^2} \ln\left(\frac{\lambda}{\xi}\right) \tag{1}$$

and the relevant current density associated is the critical current density:

$$j_c = \frac{H_{c1}}{\lambda} = \frac{\phi_0}{4\pi\mu_0\lambda(T)^3} \ln\left(\frac{\lambda}{\xi}\right) \tag{2}$$

$\lambda(T)/\xi(T)$ is the GinsburgLandau parameter, which is effectively temperature independent, and μ_0 is the magnetic permeability. The critical current density j_c should be fundamentally determined just by λ and ξ and independent of the pinning microstructure. By using in equations (1) and (2), $\lambda = 560$ nm and $\xi = 2$ nm, we obtain $B_{c1} = 28.4$ G, $j_c = 4.0 \times 10^5$ A/cm^2. This theoretical critical current density value should be compared with the extrapolated value of j_c at $T = 0$; we found for both samples $j_c \sim 1.5 \times 10^5$ A/cm^2 in good agreement with the theoretical value. The underlying physical picture is the following. When the current in the nanostrips is sufficiently high such that the component of the field normal to the strip reaches H_{c1}, vortices of opposite sign will tend to nucleate at the opposing edges and self-annihilate at the center of the nanostrips. The flux motion, in the same time, is strongly influenced by the tendency of the vortex normal cores to stay pinned to the crystalline defects of the material, a mechanism which lowers the free energy of the system. This description has to be refined because of the existence of a surface-flux line interaction effect, known as Bean Livingston barrier [27]. Even at H_{c1}, vortices may not enucleate from the edges and enter the film until a stronger field H_s (up to 20 times H_{c1} and close to the thermodynamic critical field) is reached [28]. At this field, the vortex attraction to the edge (the tendency of magnetic field lines to exit the bridge) is suppressed. Even though the average self field is considerably less than H_s, surface irregularities, defects, corners at sample ends create local fields equal or greater to H_s. These irregularities constitute preferential points of ingress for the flux lines. In particular, we argue that, in our nanostrips, the sudden increase in the cross section at the two ends of the bridge produces the current crowding

effect described by Clem *et al.* [29] and it is responsible for the observed early suppression of the superconducting state. Once inside the film, flux lines are driven inward by the Lorentz force and by the attraction of overlapping flux lines of opposite sign coming from opposite edges. The basic model of creep flow in zero external magnetic field, which we briefly review hereafter, has been specifically developed for the flux flow transistor device [19] (based on YBCO) and, more generically, in the YBCO thin film property investigations [20, 21], both based on the Kim Anderson creep flow theory [13].

Let us consider a "test" flux line inside the superconductor. The flux line motion across the strip in the x-direction induces a voltage V along the strip, at the strip terminals (see Fig. 1), which can be be written as

$$V = nLv_L\phi_0, \tag{3}$$

where n is the surface vortex density and v_L is the mean vortex velocity of flux lines crossing the strip. The average vortex density along the edges of the sample, in the absence of applied field, can be estimated from the magnetic flux density normal to the strip in correspondence with one of the two edges: $|B| \sim |\mu_0 I_b/2d|$, I_b being the bias current. Thus one obtains

$$n \sim \mu_0 I_b/(2\phi_0 d) = \mu_0 j_b w/(2\phi_0). \tag{4}$$

where we have assumed a uniform current distribution through the cross section of the nanostrip with $w < \lambda$. This way, the effect of the bias current on the voltage V is accounted for by the dependence of the vortex density on I_b. In the case of measurements in magnetic field, this dependence of the flux line density from the bias current is inessential and n is simply determined by the externally applied flux density B_a, i.e. $n \sim B_a/\phi_0$. The mean velocity in equation (3) is given by [30]

$$v_L = 2v_{L0} \exp\left(-\frac{U}{k_B T}\right) \exp\left(\frac{W}{k_B T}\right) \tag{5}$$

where v_{L0} is the maximum vortex velocity along the edges of the nanostrip, U is the pinning potential at temperature T ($U/k_B T \gg 1$), W is the work done by the mean Lorentz force $j_b d\phi_0$ during the motion of one vortex from a pinning site to the other. v_{L0} may be written in terms of δ, the effective pinning potential range, and ω_0, the attempt frequency for a magnetic flux line to hop over an energy barrier U and move a distance δ [19]

$$v_{L0} = \omega_0 \delta. \tag{6}$$

The work W can be written as $W \sim (J_b d\phi_0)\delta = I_b\phi_0\delta/w$, where $j_b = I_b/wd$ is the mean bias current density. Then the voltage equation (3) gives [19]

$$V = R_{cf} I_b \exp\left(\frac{I_b}{I_0}\right), \tag{7}$$

where $R_{cf} = (\mu_0 L\omega_0\delta/d)\exp(-U/k_BT)$, and $I_0 = wk_BT/(\delta\phi_0)$ are used as fitting parameters. R_{cf} is the resistance at low currents $\sim V/I_b$ and I_0 is related to the depairing current I_D through the relation $I_D = I_0U/k_BT$. The frequency ω_0, in the case of isolated flux lines, can be estimated by the Heisenberg relation $\omega_0\hbar \approx k_BT$ giving $\omega_0 \sim 10^{12}$Hz for $T \sim 10$K. If we assume $\delta \sim 10\xi$ (in both samples), we have for the magnetic field line velocity the value $v_{L0} \sim 2\times 10^4$ m/s. Typical measured voltage in the creep flow zone of the plot (see Fig. 5) is 0.005 V (with a current of about 30 μA (sample A) or 120 μA (sample B)). If one uses in equation (3) the above inferred v_{L0}: i.e. $v_{L0} \sim 2\times 10^4$ m/s, one obtains for the order of magnitude of the required density of flux lines, $n \sim 10^9$ (flux lines) /cm^2, corresponding to an average of ~ 80 flux lines and ~ 120 flux lines (of both signs) in sample A and B, respectively. Equation (7) is the creep flow expression used in the curve fitting shown in Fig. 5 related to the creep flow region of the CVC and introduced in the previous section.

Determining the pinning potential

In the method proposed by Enpuku [20, 21] the pinning potential is determined by measuring the temperature dependence of the CVC. Equation (7) is rewritten as

$$\begin{aligned} V &= I_b\left(\frac{\mu_0 L\omega_0\delta}{d}\right)\exp\left(-\frac{\Delta U}{k_BT}\right), \\ \Delta U(T, I_b) &= U(T) - I_b\phi_0\delta/w. \end{aligned} \tag{8}$$

where ΔU is the energy barrier against creep flow. $I_c(0)$ is the critical current at $T = 0$ and $U(T)$ is again the temperature dependent pinning potential. Now we observe [21] that the case $\Delta U \sim 0$ corresponds to a bias current $I_b = I_c(T)$ implying that $U(T) = I_c(T)\phi_0\delta/w$ or assuming the latter at $T = 0$, $I_b\phi_0\delta/w = I_bU(0)/I_c(0)$. Then equation (8) writes [20]

$$\begin{aligned} V &= A\exp(-\Delta U/k_BT), \\ \Delta U &= U(T) - I_bU(0)/I_c(0), \end{aligned} \tag{9}$$

where $A = (w\mu_0 L\omega_0/\phi_0 d)\,(U(0)/I_c(0))I_b$ is a constant independent from the temperature, in which δ does not appear any more. Next we consider the experimental values of $\log(V)$

as a function of the inverse of the temperature $1/T$ to obtain the pinning potential U by means of equation (9).

Firstly, when $T << T_c$, we assume $U(T) \sim U(0)$, and $V = A\exp(-\Delta U/k_B T)$ with $\Delta U = U(0)(1 - I_b/I_c(0))$, equation (9) becomes $V = A\exp[-U(0)(1 - I_b/I_c(0))/k_B T]$. The negative slope of the $\log(V) - 1/T$ relation can be related to the effective potential energy U_{eff} through the expression

$$U_{eff} = -k_B \frac{d(\ln(V))}{d(1/T)} = U(0)\left(1 - \frac{I_b}{I_c(0)}\right), \qquad \text{for } T << T_c, \tag{10}$$

so that $U(0) = \bar{U}_{eff} = U_{eff}|_{I_b=0}$. In Fig. 6 the experimental value of $-k_B d(\ln(V))/d(1/T)$ is shown as a function of I_b as obtained by the experimental data of Fig. 4 for the two samples A and B considering the four lowest temperatures. In agreement with equation (10), the value of $-k_B d(\ln(V))/d(1/T)$ decreases approximately linearly with I_b. This agreement shows that the flux creep dominates the CVC in the low bias current regime. From the comparison between experimental results and equation (10), illustrated in Fig. 6, we obtain the pinning potential $U(0) = \bar{U}_{eff} = 11.9$ meV for sample A, and $U(0) = \bar{U}_{eff} = 47.2$ meV for sample B. In carrying out this comparison we used the values of $Ic(0)$ obtained by the extrapolation of the $I_c - T$ relations shown in Fig. 3, that is, $I_c(0) = 76\ \mu A$ ($j_c = 1.52 \times 10^5$ A/cm^2) for sample A and $I_c(0) = 120\ \mu$A ($j_c = 1.50 \times 10^5$ A/cm^2) for sample B. The dependence from the temperature of the pinning energy $U(T)$ can be also experimentally derived by using equation (9) and dropping the condition $T \ll T_c$. One obtains [20]:

$$U(T) = U(T_1)\frac{T}{T_1} + T\int_{T_1}^{T} \frac{1}{T^2}\left[k_B \frac{d(\log V)}{d(1/T)} - U(0)\frac{I_b}{I_c(0)}\right] dT \tag{11}$$

where T_1 is an integration constant ($T_1 = 4.2$K). Again in equation (11) the value of $d(\log V)/d(1/T)$ as a function of the temperature can be experimentally obtained from the $\log(V) - 1/T$ relation shown in Fig.4. Once the integrand has been evaluated in this way, by using the previous found values of $U(0)$ and $I_c(0)$, and performing the integration in (11) numerically, we obtain the temperature dependence $U(T)$. Figure 7, a) and b), shows the result of this procedure for sample A and sample B respectively.

Correction for Nanostrips

In nanostrips with w$< \lambda$, the simultaneous presence of magnetic flux lines of opposite sign enucleated at opposite edges within a distance $l < \lambda$ must be taken into account. Indeed

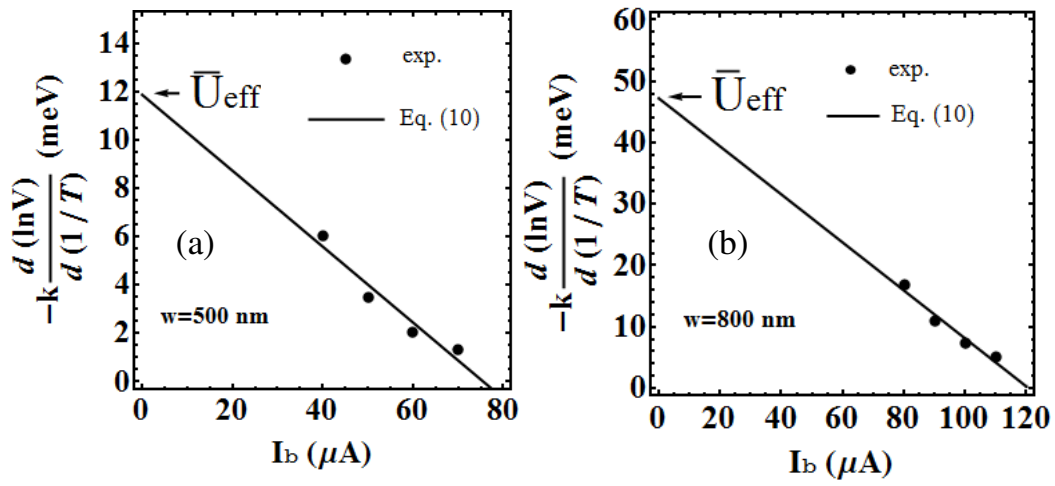

FIG. 6: Experimental relation between $d(\ln V)/d(1/T)$ and the bias current I_b, for $T \ll T_c$ for sample A, (a), and sample B, (b). The value of $d(\ln V)/d(1/T)$ is obtained from the slope of the $\log(V) - 1/T$ relation shown in Fig. 4 (a) and Fig. 4 (b), respectively. We consider the lowest four temperatures and the corresponding four experimental values of $d(\ln V)/d(1/T)$. The solid line is equation (10) with $I_c(0) = 76$ μA, $U(0) = 11.9$ meV for sample A, and $I_c(0) = 120$ μA, $U(0) = 47.2$ meV for sample B. The two values of the $I_c(0)$ were extrapolated from the experimental data illustrated in Fig. 3

there is an extra force, acting all the time and independently from the bias current, which contributes to push inward couples of magnetic flux lines with opposite sign attracting each other. This contribution adds to the work $W \sim (j_b d\phi_0)\delta$ done by the average Lorentz force and can be roughly estimated as follows. The attractive force per unit length between two vortices of opposite sign separated by l is given by [24]

$$f = \frac{\phi_0^2}{2\pi\mu_0\lambda^3} K_1\left(\frac{l}{\lambda}\right), \tag{12}$$

Sample	w(nm)	$(1+2\lambda/w)$	$I_c(0)(\mu A)$	$j_c(0)$(A/cm^2)	$\bar{U}_{eff}$(meV)	$U(0)$(meV)	δ(nm)
A	500	3.24	76	1.52×10^5	11.9	38	4
B	800	2.40	120	1.50×10^5	47.2	113	16

TABLE II: Parameters of nanostrips, U(0) is the pinning potential at T=0, corrected for W_f (Equation (17))

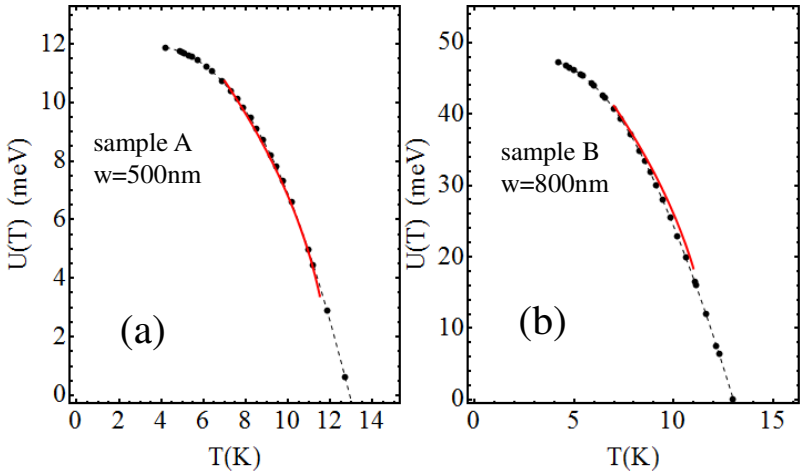

FIG. 7: Experimental result of the temperature dependence of the pinning potential U(T) for sample A, a), and B, b). The solid line in a) and b) shows the relation $U(T) = 1.4U(0)\sqrt{(T_c - T)/T_c)}$, ($T_c = 12$ K)

where K_1 is the modified Bessel function of second kind of order one. Now we assume that the two magnetic flux lines from opposite edges hop in steps of length δ towards the centre of the bridge where they self-annihilate. The interval of separation of the two flux lines ranges between a maximum $l_m \propto w$ and a minimum distance before annihilation which is approximately equal to ξ. The work done by the mean attractive force per unit length $\bar{f}$

($\bar{f} = \int_{\xi}^{l_m} f dl/(l_m - \xi)$) during the motion of one vortex from one pinning site to another is $W_f = \bar{f}\delta d$, that is

$$W_f = \delta d \frac{\phi_0^2}{2\pi\mu_0\lambda^2} \frac{K_0\left(\frac{\xi}{\lambda}\right) - K_0\left(\frac{l_m}{\lambda}\right)}{l_m - \xi} \sim \delta d \frac{\phi_0^2}{2\pi\mu_0\lambda^2} \frac{K_0\left(\frac{\xi}{\lambda}\right)}{l_m} \sim \delta d j_c \phi_0 \frac{2\lambda}{w}. \tag{13}$$

where we have used equation (2) and the approximation $K_0(\xi/\lambda) \sim \ln(\lambda/\xi)$, valid for $\lambda \gg \xi$. Note that in a large width bridge ($w \gg \lambda$) this energy contribution is small and can be neglected. We now evaluate the effect on $U(0)$ of the correction due to W_f. The barrier against creep with the introduction of $W_f = \bar{f}\delta d$ becomes

$$\Delta U(T, I_b) = U(T) - j_b \phi_0 \delta d - W_f. \tag{14}$$

The critical condition of barrier suppression against creep, $\Delta U \sim 0$ when $j_b = j_c$, gives

$$\delta = \frac{U(T)}{j_c \phi_0 d \left(1 + \frac{2\lambda}{w}\right)}. \tag{15}$$

Equation (9) generalizes to

$$\begin{aligned} V &= A \exp(-\Delta U/k_B T) \\ \Delta U &= U(T) - U(0) \frac{j_b + j_c \frac{2\lambda}{w}}{j_c \left(1 + \frac{2\lambda}{w}\right)}; \end{aligned} \tag{16}$$

where we have used equation (15) at $T = 0$. For $T \ll T_c$, we assume $U(T) \sim U(0)$ and we have

$$U_{eff} = -k \frac{d(\ln(V))}{d(1/T)} = U(0) \left(1 + \frac{2\lambda}{w}\right)^{-1} \left(1 - \frac{I_b}{I_c(0)}\right).$$

The comparison with the experimental data provides now for $U(0)$

$$U(0) = \bar{U}_{eff} \left(1 + \frac{2\lambda}{w}\right) \tag{17}$$

where again $\bar{U}_{eff} = U_{eff}|_{I_b=0}$. As summarized in Table II the obtained values of $U(0)$ are now greater, ~ 38 meV and ~ 113 meV for sample A and sample B, respectively. Nevertheless the ultimate origin of the persisting difference in values found for the pinning energy in the two samples remains unclear. Through equation (15) it is possible to estimate also the pinning potential range δ. One obtains, quite reasonably, $\delta \sim 4$ nm and $\delta \sim 16$ nm for sample A and B, respectively.

Discriminating defect types

It is interesting to compare the found $U(0)$ values with the theoretical estimates which relate the pinning energy with the kind of defect. These estimates are based on the general observation that the condensation energy $V_c\mu_0 H_c^2/2$ of a volume V_c of the vortex core can be saved if the flux line core passes through a region where the order parameter is already zero. Here H_c is the thermodynamical critical field given by $H_c = H_{c2}/\kappa\sqrt{2} = \phi_0^2/(\kappa\sqrt{2^3}\pi\mu_0\xi^2)$, where $\kappa = \lambda/\xi$ and H_{c2} is the upper critical field. For point like defects consisting of a small spherical void ($V_c \sim 4\pi/3(D/2)^3$), or non superconductive inclusion, of diameter D, smaller than the coherence length ξ, U is given by [31]

$$U = \frac{(2\pi)^{3/2} B_{c2}^{5/2}}{48\phi_0^{1/2}\kappa^2\mu_0}\xi D^3 \tag{18}$$

Even with $D = \xi$, one obtains a pinning energy as small as $U = 0.732$ meV with $B_{c2} = 100$ T, $\kappa = 560$ nm/2 nm (corresponding to a thermodynamic field $\mu_0 H_c$ of 0.25 T). That suggests a high number (order of hundreds) of small point-like type defects which pin the magnetic flux line through the thickness d of the nanostrips. For a void larger than the core region the maximum pinning energy depends on the shape and orientation of the void. For the case of a sharp void surface ($V_c \sim \pi\xi^2 L_z$) of length L_z (i.e. occupying all the thickness) parallel to the vortex, the pinning energy is given by [31]

$$U = (2\pi\phi_0)^{1/2}\frac{B_{c2}^{3/2}}{\kappa^2\mu_0}\xi L_z \tag{19}$$

which results in $U(0) = 1446$ meV for a void occupying the whole thickness of the film $L_z = d$ and with $B_{c2} = 100$ T. This suggest 2 D defects extending over a large fraction of the thickness. Assuming the temperature dependencies of H_c and ξ given by the Ginzburg-Landau theory, we obtain from equation (18) the temperature dependence of U as $U(T)/U(0) = \eta(1 - T/T_c)^{1/2}$, where η is a parameter close to one. In Fig. 7 the solid line shows the theoretical result with $\eta = 1.4$; the critical temperature has been chosen as $T_c = 12$ K (instead of 13 K) so as to fit the theoretical values to the experimental values. As can be seen, the experimental temperature dependence of U is in this way satisfactorily reproduced. Work is in progress now to study the detailed nature of U. Besides conventional mechanisms due to defects of the material, pinning originated by the interaction of fluxons with the local magnetization could be also considered in Fe(Se,Te). To this end, the

occurrence of a periodic pinning potential related to the formation of the collinear aligned spin anti-ferromagnetic order at low temperatures [32] is a stimulating theoretical possibility. Also in this case, thermally activation mechanism of the self-generated flux lines and uncorrelated motion of the flux lines can explain our experimental data.

Methods

Fe(Se,Te) highly oriented thin films base electrodes were prepared by laser ablation. A Nd:YAG laser beam at 1024 nm with 2 mm^2 spot area and fluency 0.5 J cm^{-2} is focused on the target at a repetition rate of 3 Hz. The target is positioned at 5 cm distance from the beam. Fe(Se,Te) films 100 nm thick are deposited on CaF_2 single crystal substrates. Further details may be found in refs. [33, 34].The patterning of the nanostrips has been done through two different steps. First, micrometric strips are defined by standard photolithography and ion milling etching, then the stripline dimensions are further reduced by FIB (Focused Ion Beam) using Ga-ions. For the measurements of the current-voltage characteristics the films were patterned in nanostrips $L = 3$ μm in length and width $w = 500$ nm (sample A) and $w = 800$ nm (sample B). $S_A = 5 \times 10^{-14}$ m^2 and $S_B = 8 \times 10^{-14}$ m^2 are the nominal cross section surfaces. $A_A = 1.5 \times 10^{-12}$ m^2 $A_B = 2.4 \times 10^{-12}$ m^2. The critical current density of the patterned strips at $T = 4.2$ K was $j_c = 3.2 \times 10^4$ A/cm^2 (sample A) and $j_c = 8.1 \times 10^5$A/cm^2 (sample B) (I). Current voltage characteristics have been collected in a temperature interval ranging from 4.2 K to 13 K (Sample A, 24 curves, Sample B, 27 curves) (see Fig.2). During measurements, samples are located under vacuum inside a cryogenic probe. The temperature exchange with the thermal bath is obtained with 100 mTorr helium gas. The cryogenic insert is shielded by two small concentric lead (internal) and cryoperm (external) cylinders, both at 4.2 K. Samples are measured in a highly shielded cryostat, surrounded by three μ-metal cylinders and one external aluminum shield, with an attenuation factor $S > 10^5$. Four-point contact method has been used for measuring nanostrips CVCs. Wires are filtered through low-pass passive filters, and electronics is powered with dc batteries. Samples are controlled through DAC/ADC board and data are directly collected to a PC. No external magnetic field was applied during the measurement and the presence of suitable magnetic shields granted that the superconductive transition did not originate magnetic flux trapping [35].

Acknowledgements

This work has been partially supported by the financial contribution of EU NMP.2011.2.2-6 IRONSEA Project No. 283141. FIB nanostructurations and SEM inspections have been performed at Nanofacility Piemonte INRIM, a laboratory supported by Compagnia di San Paolo Foundation.

Author contributions statement

E.S. designed the project, E. S. and C.C. performed the experiments, E.E. made the nanopatterning process, C.N. wrote the paper and made the simulations for the data analysis. E. B., V.B., and C.F. provided the thin film samples. All authors contributed to the concept and revised the manuscript.

Additional information

The authors declare no competing financial interests.

---

[1] Kamihara Y., Watanabe T., Hirano M., and Hosono H. Iron-Based Layered Superconductor La[O1-xFx]FeAs (x = 0.05-0.12) with Tc = 26 K. *Am. Chem. Soc.* 130, 3296 (2008).

[2] Paglione J. and Greene R. L., High temperature superconductivity in iron-based materials *Nature Phys.* **6** 645 (2010)

[3] Hosono H., Kuroki K., Iron-based superconductors: Current status of materials and pairing mechanism, *Physica C* **514**, 399 (2015)

[4] Mazin I. I., Singh D. J., Johannes M. D. and Du M. H. Unconventional Superconductivity with a Sign Reversal in the Order Parameter of $LaFeAsO_{1-x}F_x$ *Phys. Rev. Lett.* **101**, 057003 (2008).

[5] Nappi C., De Nicola S., Adamo M., Sarnelli E. Model prediction of high-temperatureπ-states in iron pnictide superconductor-insulator-superconductor Josephson junctions *Europhys. Lett.* **102**, 47007 (2013)

[6] Nappi C., Romeo F., Sarnelli E., Citro R. Quantum waveguide theory of the Josephson effect in multiband superconductors *Phys. Rev. B* **92**, 224503 (2015)

[7] Bellingeri E., Kawale S., Pallecchi I., Gerbi A., Buzio R., Braccini V., Palenzona A., Putti M., Adamo M., Sarnelli E., and Ferdeghini C., Strong vortex pinning in $FeSe_{0.5}Te_{0.5}$ epitaxial thin film *Applied Physics Letters* **100**, 082601 (2012)

[8] Barone C., Romeo F., Pagano S., Adamo M., Nappi C., Sarnelli E., Kurth F. and Iida K., Probing transport mechanisms of $BaFe_2As_2$ superconducting films and grain boundary junctions by noise spectroscopy, *Sci. Rep.* **4**, 6163 (2014).

[9] Barone C., Bellingeri E., Adamo M., Sarnelli E., Ferdeghini C., Pagano S. Electric field activated nonlinear 1/f fluctuations in Fe (Te, Se) superconductors, *Supercond. Sci. Technol.* **26**, 075006 (2013)

[10] Bonavolontá C., Parlato L., Pepe G. P., de Lisio C., Valentino M., Bellingeri E., Pallecchi I., Putti M. and Ferdeghini C. Ultrafast quasiparticle relaxation dynamics in high quality epitaxial $FeSe_{0.5}Te_{0.5}$ thin films *Supercond. Sci. Technol.* **26** 075018 (2013)

[11] Gao Z., Ma Y., Yao C., Zhang X., Wang C., Wang D., Awaji S. and Watanabe K. High critical current density and low anisotropy in textured $Sr_{1-x}K_xFe_2As_2$ tapes for high field applications *Sci. Rep.* **2**, 998 (2012).

[12] Talantsev E. F. and Tallon J. L. Universal self-field critical current for thin-film superconductors *Nat Commun.* **6**, 7820 (2015)

[13] Anderson P W , Y B Kim, Hard Superconductivity: Theory of the Motion of Abrikosov Flux Lines *Rev. Mod. Phys.* **36**, 39 (1962)

[14] Gurevich A., Iron-based superconductors at high magnetic fields *Rep. Prog. Phys.* **74** 124501 (2011)

[15] Lei H., Wang K., Hu R., Ryu H., Abeykoon M., Bozin E. S. and Petrovic C. Iron chalcogenide superconductors at high magnetic fields *Sci. Technol. Adv. Mater.* **13** 054305 (2012)

[16] Bellingeri E., Kawale S., Caglieris F., Braccini V., Lamura G., Pellegrino L., Sala A., Putti M., Ferdeghini C., Jost A., Zeitler U., Tarantini C. and Jaroszynski J. High field vortex phase diagram of Fe(Se, Te) thin films *Supercond. Sci. Technol.* **27** 044007 (2014)

[17] Leo A., Grimaldi G., Guarino A., Avitabile F., Nigro A., Galluzzi A., Mancusi D., Polichetti M., Pace S., Buchkov K., Nazarova E., Kawale S., Bellingeri E. and Ferdeghini C, Vortex pinning properties in Fe-chalcogenides *Superc. Sci. Technol.* **28**, 125001 (2015)

[18] Leo A., Marra P., Grimaldi G., Citro R., Shrikant K., Bellingeri E., Ferdeghini C., Pace S., and Nigro A., Competition between intrinsic and extrinsic effects in the quenching of the superconducting state in Fe(Se,Te) thin films *Phys. Rev.* B **93**, 054503 (2016)

[19] Bernstein P., Picard C., Pannetier M., Lecoeur Ph., Hamet J. F., Doan T. D., Contour J. P., Drouet M., and Regi F. X. Currentvoltage characterization of the vortex motion in $YBa_2Cu_3O_{7-\delta}$ microbridges and the implications on the development of superconducting flux flow transistors *J. App. Phys.* **82**, 5030 (1997)

[20] Enpuku K., Kisu T., Sako R., Yoshida K., Takeo M., Yamafuji K. Effect of Flux Creep on Current-Voltage Characteristics of Superconducting Y-Ba-Cu-O Thin Films *Japanese J. App.Phys.* **28** L991 (1989)

[21] Enpuku K., Sako R., Kisu T., Yoshida K., Relation between Pinning Potential and Critial Current Density of YBaCuO Superconducting Thin Films *Japanese J. Appl. Phys.* **29** L1069 (1990)

[22] Hyunsoo K., Low temperature London penetration depth and superfluid density in Fe-based superconductors. Iowa State University Graduate Theses and Dissertations. Paper 13423 (2013).

[23] Bellingeri E. 2016, private communication

[24] Orlando T. P., Delin K. A., *Foundations of applied superconductivity* (Addison-Wesley, 1991)

[25] Mannhart J, Chaudari P, Dimos D., Tsuei C. C., and McGuire T.R. Critical Currents in [001] Grains and across Their Tilt Boundaries in $YBa_2Cu_3O_7$ *Phys. Rev. Lett.* **61** 1654 (1988)

[26] Lykov A. N. Magnetic flux creep in HTSC and Anderson-Kim theory (Review Article) *Low Temp. Phys.* **40**, 773 (2014)

[27] Bean C. P., Livingston J. D. Surface Barrier in type-II Superconductors *Phys. Rev. Lett.* **12**, 14 (1964)

[28] Burlachkov L., Koshelev A. E. and Vinokur V. M. Transport properties of high-temperature superconductors: Surface vs bulk effect *Phys. Rev.* B **54** 6750 (1996)

[29] Clem J. R. and Berggren K. K. Geometry-dependent critical currents in superconducting nanocircuits *Phys. Rev.* B **84** 174510 (2011)

[30] Dew-Hughes D. Model for flux creep in high T_c superconductors *Cryogenics* **28** 674 (1988)

[31] Ullmaier H. 1975 Irreversible Properties of type II Superconductors, Springer Verlag, p 42

[32] Bao W., Qiu Y., Huang Q., Green M. A., Zajdel P., Fitzsimmons M. R., Zhemenkov M.,

Chang S., Fang M., Qian B., Vehstedt E. K., Yang J., Pharn H. M., Spinu L., Mao Z. Q., Tunable ($\delta\pi$,$\delta\pi$)-type antiferromagnetic order in α- Fe(Te,Se) superconductors, *Phys. Rev. Lett.* **102** 247001 (2009)

[33] Bellingeri E., Buzio R., Gerbi A., Marré D., Congiu S., Cimberle M. R., Tropeano M., Siri A. S., Palenzona A., and Ferdeghini C., High quality epitaxial $FeSe_{0.5}Te_{0.5}$ thin films grown on $SrTiO_3$ substrates by pulsed laser deposition *Supercond. Sci. Technol.* **22** 105007 (2009)

[34] Bellingeri E., Pallecchi I., Buzio R., Gerbi A., Marré D., Cimberle M. R., Tropeano M., Putti M., Palenzona A., and Ferdeghini C., T_c = 21 K in epitaxial $FeSe_{0.5}Te_{0.5}$ thin films with biaxial compressive strain *Appl. Phys. Lett.* **96** 102512 (2010)

[35] Stan G., Field F. B., Martinis J. M. Critical Field for Complete Vortex Expulsion from Narrow Superconducting Strips *Phys. Rev. Lett.* **92** 097003 (2004)